Global event-triggered regulation of a unicycle robot with bounded control

Mata Khalili, Denis Efimov, Shiyu Liu

Global event-triggered regulation of a unicycle robot with bounded control

Mata Khalili[a], Denis Efimov[b], Shiyu Liu[c]

[a] *Nokia Bell Labs Paris Saclay, 12 rue Jean Bart, Massy, 91300, France*
[b] *Inria, Univ. Lille, CNRS, UMR 9189 - CRIStAL, Lille, F-59000, France*
[c] *The work was conducted when Liu was at Nokia Bell Labs, France*

Abstract

This paper addresses the problem of stabilizing the position of a mobile robot using its kinematic model of unicycle type. A discontinuous and bounded control law is proposed, which guarantees a global solution to the stabilization problem. The properties of the control strategy are analyzed using Lyapunov methods. Furthermore, an event-triggered implementation of the control law is introduced, and its performance and tuning are evaluated through both simulations and experimental results.

Keywords: Event-triggered control, networked control systems, nonlinear systems

1. Introduction

The navigation problem for mobile robots admits a wide range of solutions (Kolmanovsky and McClamroch, 1995). The diversity of control laws proposed in the literature can be attributed to the presence of various constraints and performance criteria in the field of robotics (Lamnabhi-Lagarrigue, Annaswamy, Engell, Isaksson, Khargonekar, Murray, Nijmeijer, Samad, Tilbury and Van den Hof, 2017). In particular, conventional and widely adopted kinematic models for wheeled mobile robots, known as the unicycle model, are characterized by the lack of stabilizability, a facet studied in this work. For this class of dynamics, regulation of the complete state vector to a desired position via a continuous state feedback is impossible, as shown in (Brockett, 1983). As a result, several time-varying or discontinuous solutions have been proposed in the literature (de Wit, Khennouf, Samson and Sørdalen, 1994; Aicardi, Casalino, Bicchi and Balestrino, 1995; Astolfi, 1996; Jiang and Nijmeijer, 1997; Kostic, Adinandra, Caarls, Van De Wouw and Nijmeijer, 2009). One common approach to address this structural challenge is to shift the focus from stabilization to tracking (d'Andréa Novel, Campion and Bastin, 1995; De Luca, Oriolo and Samson, 1998), which inherently introduces time-varying control. Another approach relaxes the regulation objective by requiring control of the robot's position only, rather than both position and orientation at the final destination. This relaxation makes continuous feedback feasible (Dixon, Dawson, Zergeroglu and Behal, 2001).

An important characteristic in practical applications is the boundedness of the control input, since robot motors cannot generate arbitrarily large torques. This becomes a challenging issue when global regulation (or regulation under sufficiently large deviations) is considered, as noted in (Evers and Nijmeijer, 2006; Do, 2013; Martínez, Ríos and Mera, 2021). Note that most existing control laws are either not bounded or not global, or their applicability is based on rather sophisticated hypotheses.

In the case of long-range navigation of a mobile robot, where a centralized planner provides unified supervision of a fleet of heterogeneous agents, an additional important constraint arises: the network load imposed by control and estimation algorithms. Extensive use of the communication channel by various distributed navigation and monitoring tools and agents may lead to channel saturation and packet losses, resulting in degraded quality of service and significant delays (Tatikonda and Mitter, 2004).

One strategy to alleviate network load is sampled or event-triggered (ET) control and estimation (Tabuada, 2007; Lemmon, 2010; Girard, 2015; Postoyan, Tabuada, Nešić and Anta, 2015b), where information is updated only when certain conditions are violated. This approach guarantees proper and desirable system performance. A popular and simple method for embedding existing feedback solutions to an ET setup relies on the use of a Lyapunov function, which ensures stability of the control in the continuous-time case (Postoyan, Bragagnolo, Galbrun, Daafouz, Nešić and Castelan, 2015a; Zhang, Liu and Jiang, 2023).

In this work, we address the problem of global position regulation to a point for a disturbed unicycle, without imposing a final constraint on its orientation, under bounded control, followed by its extension to the ET framework using the method of (Postoyan et al., 2015b). In mobile robotics, navigation is typically structured around two levels of planning: a global planner, which computes a feasible path to the goal, and a local planner, which generates control commands to follow that path while avoiding dynamic

obstacles (Fox, Burgard and Thrun, 1997; Kuwata, Teo, Fiore, Karaman, Frazzoli and How, 2009). Consistent with this structure, we assume that the global planner provides a sequence of waypoints that the robot has to follow in a given order. There are no strict requirements on the robot's behavior between waypoints, which facilitates integration of this control strategy with collision avoidance algorithms. In contrast to trajectory tracking, where a collision avoidance maneuver may require replanning the entire trajectory, the waypoint-based approach avoids intervention from the global planner, thereby saving computational and communication resources.

The use of bounded control allows the robot to navigate globally while staying close to its maximal admissible velocity, especially when the control signal is saturated across most of the operating domain. At the same time, the ET framework minimizes communication load, as described above.

To this end, we first propose a discontinuous bounded global robust stabilizer of the position control with a strict Lyapunov function (the discontinuity region is not transgressed during the transients, thus, the control signal remains continuous along each particular trajectory). The stabilization problem is solved in the presence of matched disturbances. Secondly, following the approach from (Postoyan et al., 2015b), an ET scheme is formulated. Finally, the tuning of the control parameters is carried out using simulation (with the outcomes detailed in (Efimov, Khalili and Liu, 2024)), while the performance of ET regulation is evaluated through extensive simulations in Gazebo and experimental validation.

The remainder of this paper is organized as follows. The problem statement is presented in Section 2. The design of a bounded global stabilizer for the unicycle's position is given in Section 3, where the analysis is based on Lyapunov methods. An ET implementation of the proposed bounded feedback is investigated in Section 4. The tuning of the control parameters and their influence on the transients are examined by computer simulations and discussed in Section 5. Finally, Section 6 demonstrates the control performance of the ET scheme through real-world experiments.

Notation

Denote by $\mathbb{R}$ and $\mathbb{Z}$ the sets of real numbers and integers, respectively, $\mathbb{Z}_+ = \{j \in \mathbb{Z} : j \geq 0\}$.

The symbol $|\cdot|$ denotes the absolute value of a real.

The definitions of the stability properties and notions used in this work can be found in (Khalil, 2002).

2. Problem statement

Consider a mobile robot, whose dynamics are described by the unicycle kinematic model:

$$\begin{aligned} \dot{x}(t) &= u_1(t)(1 + d_1(t))\cos(\theta(t)), \\ \dot{y}(t) &= u_1(t)(1 + d_1(t))\sin(\theta(t)), \\ \dot{\theta}(t) &= u_2(t)(1 + d_2(t)), \end{aligned} \tag{1}$$

where $x(t), y(t) \in \mathbb{R}$ determine the robot's position in the plane, and $\theta(t) \in [-\pi, \pi)$ is the heading angle that tabulates the orientation, $X(t) = [x(t), y(t), \theta(t)]^\top$ denotes the state vector of the system; $u_1(t) \in [-u^1_{\max}, u^1_{\max}], u_2(t) \in [-u^2_{\max}, u^2_{\max}]$ are bounded controls corresponding to the linear and angular velocities, respectively, with $u^1_{\max} > 0$ and $u^2_{\max} > 0$ denoting the maximal admissible control amplitudes, $U(t) = [u_1(t), u_2(t)]^\top$; $-1 < -\bar{d}_i \leq d_i(t) \leq \bar{d}_i$ for $i = 1, 2$ represent disturbances in the respective control channels, with known bounds $\bar{d}_i$; $t \geq 0$. The assumption that $\bar{d}_i < 1$, $i = 1, 2$ means that the disturbance cannot change the direction of the movement of the robot, while the multiplicative nature of these perturbations implies that if the controls $u_i(t) \equiv 0$, then the disturbance $d_i(t)$ alone cannot force the robot to move.

Problem. Design a bounded ET state feedback $u_1(t) = u_1(X(t))$ and $u_2(t) = u_2(X(t))$ that globally stabilizes any given neighborhood of the set $\mathcal{O} = \{X \in \mathbb{R}^2 \times [-\pi, \pi) : x = y = 0\}$ for system (1) with $|d_i(t)| \leq \bar{d}_i$, $i = 1, 2$ for all $t \geq 0$.

The solution proceeds in two steps: first, a global bounded discontinuous feedback robustly stabilizing $\mathcal{O}$ for (1) will be synthesized (the angle θ is not constrained when the position $x = y = 0$ is reached); second, an ET mechanism will be proposed using the Lyapunov function methodology, following (Postoyan et al., 2015a). Note that the practical regulation of the set $\mathcal{O}$ is demanded in order to avoid an infinite commutation approaching this set (the effect of the disturbances d_1 and d_2 should be completely counteracted by the control); if Zeno behavior is admissible, then the same ET control can guarantee the exact asymptotic convergence to $\mathcal{O}$.

3. Global bounded position stabilizer

In this section, we propose a bounded state feedback $U(X)$ providing asymptotic stability of the closed-loop system at $\mathcal{O}$ uniformly in $|d_i(t)| \leq \bar{d}_i$, $i = 1, 2$ for all $t \geq 0$.

Let us define the desired orientation of the robot as

$$\theta_d(t) = \arctan\left(\frac{y(t)}{x(t)}\right) - \pi,$$

then the heading $\theta(t) = \theta_d(t)$ implies that the robot is oriented precisely toward the point $x = y = 0$ (further, in this section the time dependence

of the variables will be omitted for brevity). Recalling the formulas $\cos(\arctan(\phi)) = \frac{1}{\sqrt{1+\phi^2}}$ and $\sin(\arctan(\phi)) = \frac{\phi}{\sqrt{1+\phi^2}}$ which hold for any $\phi \in \mathbb{R}$, the following useful equalities can be established:

$$\begin{aligned} x\cos(\theta_d) + y\sin(\theta_d) &= -\sqrt{x^2+y^2}, \\ x\sin(\theta_d) - y\cos(\theta_d) &= 0. \end{aligned} \tag{2}$$

To design the control laws, we employ a simple quadratic Lyapunov function:

$$V(X) = x^2 + y^2 + \gamma(\theta - \theta_d)^2,$$

where $\gamma > 0$ is a design parameter whose role will be clarified in the next section. The function V is continuous and positive definite for $\theta - \theta_d \in [-\pi, \pi)$ (*i.e.*, $V(X) = 0$ implies $X \in \mathcal{O}$), but it is not continuously differentiable for $|\theta - \theta_d| \to \pi$. Calculating the derivative of V along the trajectories of (1), we obtain:

$$\begin{aligned} \dot{V} &= 2x\dot{x} + 2y\dot{y} + 2\gamma(\theta - \theta_d)(\dot{\theta} - \dot{\theta}_d) \\ &= 2(1+d_1)u_1(x\cos(\theta) + y\sin(\theta)) \\ &\quad +2\gamma(\theta - \theta_d)((1+d_2)u_2 - \dot{\theta}_d), \end{aligned} \tag{3}$$

where straightforward computations show that:

$$\dot{\theta}_d = (1+d_1)u_1 \frac{x\sin(\theta) - y\cos(\theta)}{x^2+y^2}. \tag{4}$$

Let us select the control laws in the form:

$$u_1(X) = -\rho(\theta - \theta_d)\varphi_1\left(k_1(x\cos(\theta) + y\sin(\theta))\right), \tag{5}$$

$$u_2(X) = -\varphi_2\left(k_2(\theta - \theta_d) - \frac{\dot{\theta}_d}{u^2_{\max}}\right),$$

where,

$$\varphi_i(s) = u^i_{\max}\begin{cases} s & \text{if } |s| \le 1 \\ \text{sign}(s) & \text{if } |s| > 1 \end{cases}, \; i = 1,2,$$

$$\rho(s) = \exp(-\eta s^2),$$

and $k_1 > 0$, $k_2 > 0$, and $\eta > 0$ are tuning gains, whose values will be constrained later. Note that the control u_2 may be discontinuous as $|\theta - \theta_d| \to \pi$.

Remark 1. The intuition behind the appearance of ρ is to decrease the linear velocity of the robot u_1 for large deviations of θ from its desired value θ_d (and when the control u_1 in (5) takes negative values), which can be regulated by adjusting the value of η. The gains k_1 and k_2 enlarge the domain in which the maximum amplitude of the control $u^i_{\max}$, $i = 1,2$ is applied by (5).

By construction, the following properties are satisfied for all $X \in \mathbb{R}^2 \times [-\pi, \pi)$:

$$\begin{aligned} 0 < \exp(-\eta\pi^2) \le \rho(\theta - \theta_d) \le 1, \\ -u^i_{\max} \le \varphi_i(s) \le u^i_{\max}, \; i = 1,2, \; \forall s \in \mathbb{R}, \end{aligned}$$

hence, the control values belong the admissible sets:

$$-u^i_{\max} \le u_i(X) \le u^i_{\max}, \; i = 1,2.$$

Moreover, several less obvious relations can be established:

Lemma 1. *For any* $X \in \mathbb{R}^2 \times [-\pi, \pi)$,

$$|\dot{\theta}_d| \le \kappa_{\max}|\theta - \theta_d|$$

with $\kappa_{\max} = \sqrt{2}k_1(1+\bar{d}_1)u^1_{\max}$.

Proof. Subtracting the second equality in (2) from the numerator of (4) we obtain:

$$\begin{aligned} |\dot{\theta}_d| &= (1+d_1)|u_1| \\ &\times \frac{|x(\sin(\theta) - \sin(\theta_d)) + y(\cos(\theta_d) - \cos(\theta))|}{x^2+y^2} \\ &\le (1+\bar{d}_1)|u_1|\frac{|x|+|y|}{x^2+y^2}|\theta - \theta_d|, \end{aligned}$$

where we used inequalities:

$$|\sin(\theta) - \sin(\theta_d)| \le |\theta - \theta_d|, \; |\cos(\theta_d) - \cos(\theta)| \le |\theta - \theta_d|.$$

Standard relations between vector norms yield

$$\frac{1}{\sqrt{x^2+y^2}} \le \frac{|x|+|y|}{x^2+y^2} \le \frac{\sqrt{2}}{\sqrt{x^2+y^2}}.$$

Note that $|u_1| = \rho(\theta - \theta_d)u^1_{\max}$ for $|k_1(x\cos(\theta) + y\sin(\theta))| \ge 1$. Introducing the polar coordinates $r = \sqrt{x^2+y^2}$ and $\psi \in [-\pi, \pi)$ for the variables $x \in \mathbb{R}$ and $y \in \mathbb{R}$ we obtain $x = r\cos(\psi)$ and $y = r\sin(\psi)$. Hence, $|k_1(x\cos(\theta) + y\sin(\theta))| = rk_1|\cos(\psi)\cos(\theta) + \sin(\psi)\sin(\theta)| = rk_1|\cos(\theta - \psi)| \ge 1$ implies the necessary condition: $\sqrt{x^2+y^2} \ge k_1^{-1}$. Therefore, for $|k_1(x\cos(\theta) + y\sin(\theta))| \ge 1$,

$$\begin{aligned} |u_1|\frac{|x|+|y|}{x^2+y^2} &\le \rho(\theta - \theta_d)u^1_{\max}\frac{\sqrt{2}}{\sqrt{x^2+y^2}} \\ &\le \sqrt{2}k_1u^1_{\max}\rho(\theta - \theta_d), \end{aligned}$$

while otherwise, for $|k_1(x\cos(\theta) + y\sin(\theta))| < 1$

$$\begin{aligned} &|u_1|\frac{|x|+|y|}{x^2+y^2} \\ &\le \rho(\theta - \theta_d)u^1_{\max}|k_1(x\cos(\theta) + y\sin(\theta))|\frac{\sqrt{2}}{\sqrt{x^2+y^2}} \\ &= \rho(\theta - \theta_d)u^1_{\max}\sqrt{x^2+y^2}k_1|\cos(\theta - \psi)|\frac{\sqrt{2}}{\sqrt{x^2+y^2}} \\ &\le \sqrt{2}k_1u^1_{\max}\rho(\theta - \theta_d), \end{aligned}$$

which proves the lemma, taking into account that $\rho(\theta - \theta_d) \le 1$. □

Lemma 2. *There exists* $\eta > 0$ *such that*

$$|\dot{\theta}_d| \le \kappa_{\min} < (1 - \bar{d}_2)u^2_{\max} \tag{6}$$

for all $x \in \mathbb{R}$, $y \in \mathbb{R}$ *and all* $|\theta-\theta_d| \geq \frac{1}{k_2+(u^2_{\max})^{-1}\kappa_{\max}}$, *where*

$$\kappa_{\min} = \kappa_{\max} \max\left\{ \frac{\exp(-0.5)}{\sqrt{2\eta}}, \frac{\exp\left(\frac{-\eta}{(k_2+(u^2_{\max})^{-1}\kappa_{\max})^2}\right)}{k_2+(u^2_{\max})^{-1}\kappa_{\max}} \right\}$$

Proof. As shown above,

$$\begin{aligned} |\dot\theta_d| &\leq \kappa_{\max}\rho(\theta-\theta_d)|\theta-\theta_d| \\ &= \sqrt{2}k_1(1+\bar d_1)u^1_{\max}\exp\left(-\eta|\theta-\theta_d|^2\right)|\theta-\theta_d| \end{aligned}$$

for all $X \in \mathbb{R}^2 \times [-\pi,\pi)$, and $f(s) = \exp\left(-\eta s^2\right)s$ for $s \geq 0$ admits the maximal value $f_{\max} = \frac{\exp(-0.5)}{\sqrt{2\eta}}$ for $s = s_{\max} = \frac{1}{\sqrt{2\eta}}$, moreover, $\lim_{s\to 0} f(s) = 0$ and $\lim_{s\to+\infty} f(s) = 0$. Therefore,

$$|\dot\theta_d| \leq \kappa_{\min}$$

for all $x \in \mathbb{R}$, $y \in \mathbb{R}$ and all $|\theta-\theta_d| \geq \frac{1}{k_2+\frac{\kappa_{\max}}{u^2_{\max}}}$, and the upper bound above can be made arbitrary small by tuning the value of η, *i.e.*,

$$|\dot\theta_d| < (1-\bar d_2)u^2_{\max}$$

in this range of state variables if

$$\eta > \max\Bigg\{ \exp(-1)\left(\frac{k_1(1+\bar d_1)u^1_{\max}}{(1-\bar d_2)u^2_{\max}}\right)^2, \quad (7)$$
$$-\left(k_2+\frac{\kappa_{\max}}{u^2_{\max}}\right)^2 \ln\left((1-\bar d_2)\left(1+u^2_{\max}\frac{k_2}{\kappa_{\max}}\right)\right)\Bigg\},$$

and the result follows. □

Now, we substitute the controls (5) into the derivative (3) of V and obtain the conditions guaranteeing its negative definiteness:

$$\begin{aligned} \dot V = &-2\rho(\theta-\theta_d)(1+d_1)\varphi_1\left(k_1(x\cos(\theta)+y\sin(\theta))\right) \\ &\times(x\cos(\theta)+y\sin(\theta)) \\ &-2\gamma(\theta-\theta_d)\left[(1+d_2)\varphi_2\left(k_2(\theta-\theta_d)-\frac{\dot\theta_d}{u^2_{\max}}\right)+\dot\theta_d\right]. \end{aligned}$$

By construction, the first term is negative definite in $x\cos(\theta)+y\sin(\theta)$ (*i.e.*, $\rho(\xi)\varphi_1(k_1\zeta)\zeta \geq u^1_{\max}\exp(-\eta\pi^2)\min\{|\zeta|, k_1\zeta^2\}$ for any $\zeta \in \mathbb{R}$ and $\xi \in [-\pi,\pi)$). For the second term, two cases must be considered: 1) if $|k_2(\theta-\theta_d)-(u^2_{\max})^{-1}\dot\theta_d| \leq 1$, then

$$\begin{aligned} &(\theta-\theta_d)\left[(1+d_2)\varphi_2\left(k_2(\theta-\theta_d)-\frac{\dot\theta_d}{u^2_{\max}}\right)+\dot\theta_d\right] \\ &= (1+d_2)u^2_{\max}k_2(\theta-\theta_d)^2 - d_2(\theta-\theta_d)\dot\theta_d \\ &\geq (1-\bar d_2)u^2_{\max}k_2(\theta-\theta_d)^2 - \bar d_2\kappa_{\max}(\theta-\theta_d)^2 \geq 0 \end{aligned}$$

provided that

$$(1-\bar d_2)u^2_{\max}k_2 > \bar d_2\kappa_{\max}$$

or equivalently,

$$k_2 > \sqrt{2}\bar d_2 k_1 \frac{(1+\bar d_1)u^1_{\max}}{(1-\bar d_2)u^2_{\max}};$$

2) if $|k_2(\theta-\theta_d)-(u^2_{\max})^{-1}\dot\theta_d| > 1$, then recalling the result of Lemma 1 we obtain that for

$$k_2 > (u^2_{\max})^{-1}\kappa_{\max} = \sqrt{2}k_1(1+\bar d_1)\frac{u^1_{\max}}{u^2_{\max}}$$

the term $k_2(\theta-\theta_d)$ dominates $(u^2_{\max})^{-1}\dot\theta_d \leq (u^2_{\max})^{-1}\kappa_{\max}|\theta-\theta_d|$ and $\operatorname{sign}(k_2(\theta-\theta_d) - (u^2_{\max})^{-1}\dot\theta_d) = \operatorname{sign}(\theta-\theta_d)$. Both restrictions on k_2 can be combined as

$$k_2 > \sqrt{2}k_1 \max\left\{1, \frac{\bar d_2}{1-\bar d_2}\right\}\frac{(1+\bar d_1)u^1_{\max}}{u^2_{\max}}, \quad (8)$$

then

$$\begin{aligned} &(\theta-\theta_d)\left[(1+d_2)\varphi_2\left(k_2(\theta-\theta_d)-\frac{\dot\theta_d}{u^2_{\max}}\right)+\dot\theta_d\right] \\ &= (\theta-\theta_d)\left[(1+d_2)u^2_{\max}\operatorname{sign}(\theta-\theta_d)+\dot\theta_d\right]. \end{aligned}$$

Moreover, under (8), $(k_2+(u^2_{\max})^{-1}\kappa_{\max})|\theta-\theta_d| > 1$ necessarily follows from $|k_2(\theta-\theta_d)-(u^2_{\max})^{-1}\dot\theta_d| > 1$, which implies that in this case $|\theta-\theta_d| \geq \frac{1}{k_2+(u^2_{\max})^{-1}\kappa_{\max}}$ and due to Lemma 2 (with η properly selected from (7)):

$$|\dot\theta_d| \leq \kappa_{\min} < (1-\bar d_2)u^2_{\max}.$$

Finally we derive:

$$\begin{aligned} &(\theta-\theta_d)\left[(1+d_2)\varphi_2\left(k_2(\theta-\theta_d)-\frac{\dot\theta_d}{u^2_{\max}}\right)+\dot\theta_d\right] \\ &\geq (1-\bar d_2)u^2_{\max}|\theta-\theta_d| - \kappa_{\min}|\theta-\theta_d| \geq 0. \end{aligned}$$

Combining these facts, we conclude that $\dot V < 0$ for all $x^2+y^2 \neq 0$ and $\theta \neq \theta_d$, which ensures boundedness of the state X and global asymptotic convergence of all trajectories in (1), (5) to the set $\mathcal{O}$ uniformly in the disturbances $|d_i| \leq \bar d_i$, $i = 1,2$. Note that the line $\theta = \theta_d \pm \pi$ is not transgressed by the trajectories of the closed-loop system, hence, there is no problem with discontinuity of the control u_2 (the solutions are well defined and no chattering occurs).

Therefore, the following result has been proven:

Theorem 1. *For any given* $u^i_{\max}$, $i = 1,2$ *and* $k_1 > 0$, *let* $k_2 > 0$ *be chosen to satisfy* (8) *while* $\eta > 0$ *to guarantee* (6), *then all trajectories of* (1) *(with* $|d_i(t)| \leq \bar d_i$, $i = 1,2$ *for all* $t \geq 0$*),* (5) *are bounded and the set* $\mathcal{O}$ *is the global asymptotic attractor in* $X \in \mathbb{R}^2 \times [-\pi,\pi)$.

The proof of this theorem indicates that by increasing the values of $u^i_{\max}$ or k_i, $i = 1,2$ it is possible to accelerate the convergence speed in the system, whereas the value of η is best kept as small as possible in accordance with the bound derived in the proof of Lemma 2.

Remark 2. Note that the restrictions obtained for the values of $\kappa_{\max}$, $\kappa_{\min}$, k_2 and η are very conservative and they mainly indicate the reasons why these quantities exist. For implementation purposes, it is better to adjust them based on numerical experiments (using the trial and error method). The only necessary relations are

$$k_2 > (u_{\max}^2)^{-1}\kappa_{\max},\ \kappa_{\min} < (1-\bar{d}_2)u_{\max}^2,$$

where $\kappa_{\max}$ and $\kappa_{\min}$ are the bounds on $|u_1|\frac{|x|+|y|}{x^2+y^2}$ and $|\dot{\theta}_d|$ for $X \in \mathbb{R}^2 \times [-\pi,\pi)$ and $|\theta-\theta_d| \geq \frac{1}{k_2+(u_{\max}^2)^{-1}\kappa_{\max}}$, respectively.

4. Event-triggering regulation

Let us consider how the control (5) can be implemented within the event-triggered framework.

Assume that the control of the robot (1) is realized through a sampling-and-hold mechanism. Thus, there exists a sequence of time instants t_k, $k \in \mathbb{Z}_+$ such that $t_{k+1} > t_k \geq t_0 = 0$ and $u_i(t) = u_i(t_k)$ for all $t \in [t_k, t_{k+1})$. The regulation problem stays the same, that is stabilization of any given neighborhood of the set $\mathcal{O}$. We assume that the instants t_k can be selected by the designed ET mechanism, whose objective is to minimize the number of switchings (commutations) during the transients.

Recalling the properties of the control (5) established in the proof of Theorem 1, we obtain the following property:

$$\begin{aligned}\dot{V} &= 2[(1+d_1)u_1(x\cos(\theta)+y\sin(\theta))\\ &\quad +\gamma(\theta-\theta_d)((1+d_2)u_2-\dot{\theta}_d)]\\ &\leq 2[(1-\bar{d}_1)u_1(x\cos(\theta)+y\sin(\theta))\\ &\quad +\gamma(\theta-\theta_d)((1-\bar{d}_2)u_2-\dot{\theta}_d)]\\ &:= W(X,U),\end{aligned}$$

where the function W depends only on known variables and parameters.

According to conventional ET results (Postoyan et al., 2015b,a), let us select the following supervision algorithm for $\sqrt{x^2(t_k)+y^2(t_k)} > \varepsilon$:

$$\begin{aligned}t_{k+1} = \arg\inf_{t>t_k}\{&\sqrt{x^2(t)+y^2(t)} \leq \varepsilon \text{ or } W(X(t),U(t_k))\\ &\geq \alpha W(X(t),U(t))\},\end{aligned} \tag{9}$$

where $\varepsilon > 0$ and $\alpha \in (0,1]$ are tuning parameters, W is defined above and $U(t) = [u_1(X(t)), u_2(X(t))]^\top$ is given by (5). Here, $X(t)$ denotes the current state measurement, and

$$U(t_k) = \begin{cases} \begin{bmatrix} 0 \\ 0 \end{bmatrix} & \text{if } \sqrt{x^2(t_k)+y^2(t_k)} \leq \varepsilon \\ \begin{bmatrix} u_1(X(t_k)) \\ u_2(X(t_k)) \end{bmatrix} & \text{otherwise} \end{cases}, \tag{10}$$

where again u_1 and u_2 are defined in (5). In the control (9), (10), ε determines the neighborhood of the set $\mathcal{O}$ that is stabilized, then the control (the robot velocities) is set to zero once it is reached. During the transients, the derivative of the Lyapunov function V, calculated in (3) for the frozen control $W(X(t),U(t_k))$ is compared with the one obtained for (1), (5), namely $W(X(t),U(t))$ assuming that the disturbances take their worst case values; if $W(X(t),U(t_k)) < \alpha W(X(t),U(t)) \leq 0$ then the new event is not generated and the triggered control is not updated (according to Theorem 1 we know that $W(X(t),U(t))$ is negative for any $x^2(t)+y^2(t) \neq 0$ and $\theta(t) \neq \theta_d(t)$, hence, $W(X(t),U(t_k))$ is guaranteed to remain negative). The parameter α characterizes the admissible deviation in the decay of $V(t)$ by $U(t_k)$ with respect to that provided by the nominal control law $U(t)$.

Since $\varepsilon > 0$ and $\alpha > 0$, and $-W(X(t),U(t))$ admits a lower bound as a function of the distance to the set $\mathcal{O}$, i.e., in terms of $\sqrt{x^2(t)+y^2(t)}$, then $t_{k+1} > t_k$ and the Zeno behavior is impossible.

Theorem 2. *Assume that all conditions of Theorem 1 are satisfied, then for any $\varepsilon > 0$ and $\alpha > 0$ all trajectories in* (1) *with the triggered control defined by* (9) *and* (10) *remain bounded, and there exists a finite index $k^* = k^*(X(0)) \geq 0$ such that $\sqrt{x^2(t_{k^*})+y^2(t_{k^*})} \leq \varepsilon$.*

Proof. Under the conditions of Theorem 1, $W(X(t),U(t)) < 0$ for $\sqrt{x^2(t)+y^2(t)} > \varepsilon$. Hence, $W(X(t),U(t_k)) < 0$ while $\sqrt{x^2(t)+y^2(t)} > \varepsilon$ for all $k \in \mathbb{Z}_+$ by (9), which due to the properties of the Lyapunov function V, implies the existence of k^* as desired. □

The role of the parameter γ introduced in V consists in weighting the angle regulation term $(\theta-\theta_d)^2$ relative to the positioning component of V to generate the control scheduling in (9) providing reasonable deviations of the trajectories from the nominal ones. The former term is globally bounded by $2\gamma\pi(u_{\max}^2+\kappa_{\max}\pi)$ for $\theta-\theta_d \in [-\pi,\pi)$, while the latter can be unbounded for $x, y \in \mathbb{R}$.

5. Simulation-based tuning of event-triggered control parameters

To determine the optimal values of the ET parameters α and γ, and to assess their impact on controller performance and the triggering frequency of control commands, preliminary simulations were conducted with the Clearpath Jackal robot in Gazebo using ROS 1 Noetic. The maximum linear and angular velocities of the robot were limited to 0.5 m/s and 1 rad/s respectively, values that are commonly used in dynamic indoor spaces where robots share the environment with humans and other moving objects to ensure safe operation. The stopping threshold

ϵ was set to 0.1 m, a reasonable choice considering the robot's physical dimensions (0.5×0.43 m), and the same value was used across all simulations and experiments for comparability.

Tuning was carried out under the following conditions:

- **Waypoint spacing (d):** Distances of 0.5 m, 2 m, and 5 m were tested, covering both fine maneuvers (e.g., for obstacle avoidance) and coarse movements for long-distance navigation.
- **Initial heading deviation ($\tilde{\theta}_{init}$)[1]:** Deviations of 5°, 60°, 120°, and 180° were evaluated, representing cases where the robot is nearly aligned, moderately deviating, strongly deviating, or facing away from its next waypoint (the goal).

For each simulation scenario, the control parameters (k_1, k_2, and η) were taken from a lookup table based on previous results (Efimov et al., 2024), ensuring best performing settings for each waypoint spacing and initial heading deviation. The localization system in the simulation relied on LiDAR, with the Laser Scan Matcher (LSM) method (Censi, 2008). The environment replicated the Unix maze space at Nokia Bell Labs in Murray Hill, named after the large UNIX letters forming the maze walls, creating a realistic and challenging test scenario with both open areas and narrow pathways with tight corners, as illustrated in Figure 1. During parameter tuning, disturbances in (9) were neglected (i.e., $\bar{d}_1 = \bar{d}_2 = 0$) to isolate parameter effects and identify optimal values without external influences on controller performance.

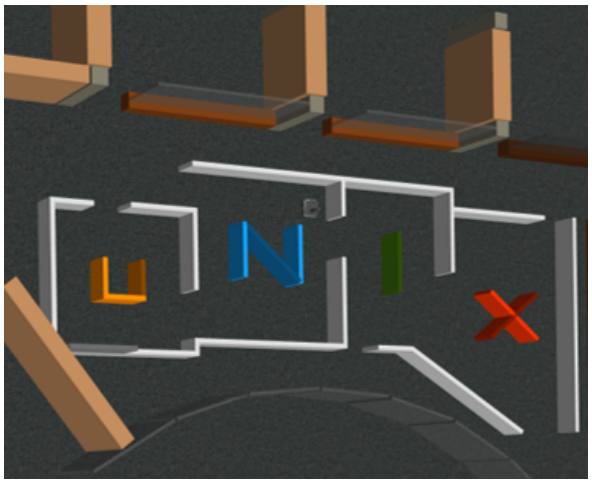

Figure 1: The Unix maze environment in Gazebo used for simulations, featuring open areas and narrow pathways with tight corners.

The α parameter was varied in steps of 0.1 over $[0.1, 1.0]$, while γ was chosen from $\{1, 5, 10, 20\}$, following prior simulations that identified these as effective settings. This comprehensive sweep enabled evaluation of the influence of α and γ under diverse initial conditions. Each configuration was tested 10 times for every waypoint spacing, initial heading deviation, and ET parameter combination.

To study the relationship between parameter variation and controller performance, the correlations of α and γ with the Heading, Distance, and Speed Indicators were analyzed across different waypoint distances and initial heading deviations as shown in Figure 2. These indicators were originally introduced in (Efimov et al., 2024), and are recalled here for completeness:

1. **Heading indicator**. This metric measures the accumulated heading corrections normalized by the expected initial correction. It evaluates both the rate at which the robot aligns its heading toward the goal and the smoothness of heading variation along the trajectory:

$$m_h = \frac{1}{|\tilde{\theta}_{init}|} \int_0^T |\theta(t) - \theta^{\mathrm{d}}(t)| dt,$$

   where $|\theta(t) - \theta^{\mathrm{d}}(t)|$ is the instantaneous deviation in heading from the intended direction to the goal. The notation $|\theta|$ denotes the wrapped angle norm within $[-\pi, \pi)$.

2. **Distance indicator**. This metric quantifies the deviation of the robot's trajectory from the straight line connecting two waypoints. It reflects the spatial footprint of the robot's motion as well as the smoothness of the path. It is defined as

$$m_d = \frac{s}{d},$$

   where d is the shortest distance between two waypoints.

3. **Speed indicator**. This metric evaluates the average speed of the robot when traveling between waypoints relative to the maximum admissible velocity. It is defined as

$$m_s = \frac{s}{T\, u^1_{\max}},$$

   where s is the total traveled distance and T is the travel time.

Together, these metrics provide complementary insights into: (i) the rate and smoothness of heading alignment, (ii) the degree of deviation from the nominal path, and (iii) the average speed relative to the velocity limit (Efimov et al., 2024).

We compute Pearson correlations between the design parameters α and γ and each metric–distance m_d and heading m_h (lower are better), and speed m_s (higher is better)–pooled across waypoint spacings d and initial heading deviations $\tilde{\theta}_{\mathrm{init}}$. This analysis

[1] $|\theta_{init} - \theta^{\mathrm{d}}_{init}| := \tilde{\theta}_{init}$ denotes the angular deviation between the initial and desired heading when the robot is directed towards the goal, as described in (Efimov et al., 2024).

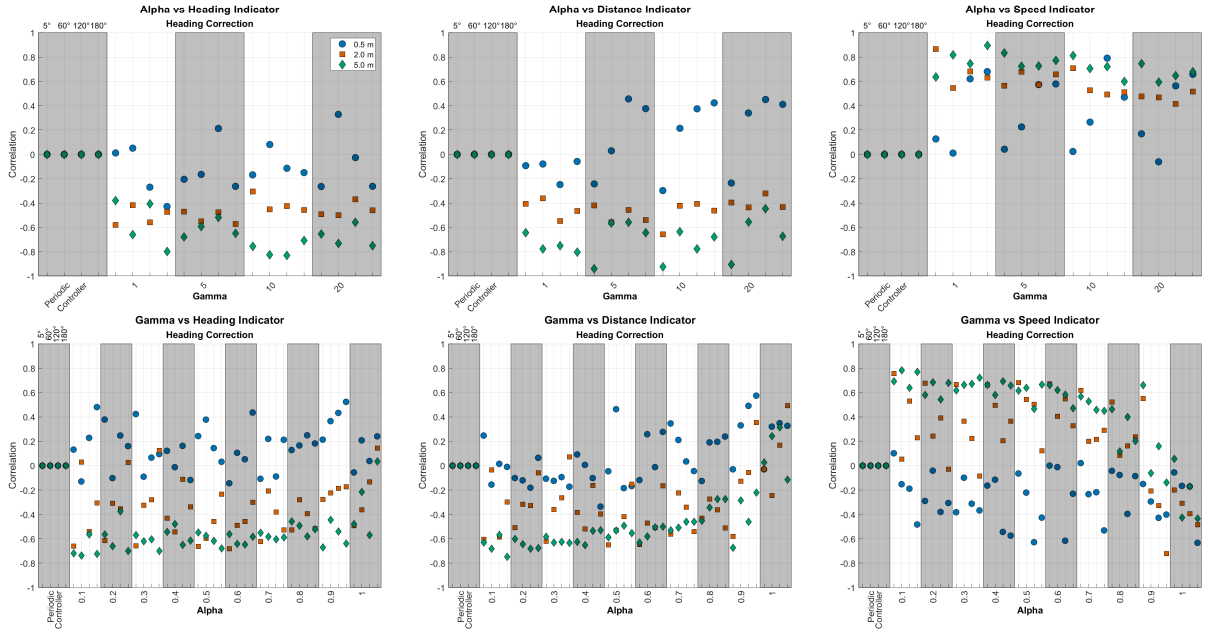

Figure 2: Correlation coefficients between tuning parameters α and γ and performance indicators (heading m_h, distance m_d, speed m_s) across waypoint spacings $d \in \{0.5, 2, 5\}$ m and initial heading deviations $\tilde{\theta}_{\text{init}} \in \{5°, 60°, 120°, 180°\}$.

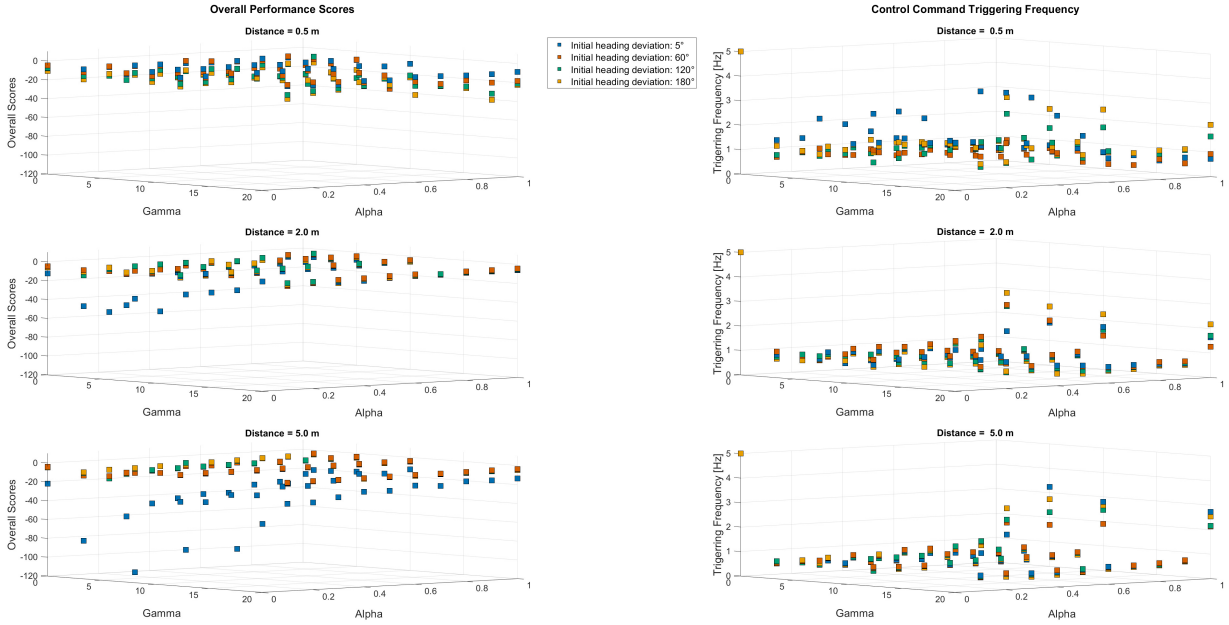

Figure 3: Preliminary simulation results across the tested conditions. Right: overall performance score. Left: control command triggering frequency, which indicates the communication load (lower triggering frequency implies reduced communication load).

serves to (i) reveal the direction and relative strength of association for each parameter metric pair, (ii) identify trade-offs (e.g., settings that raise m_s but worsen m_d or m_h), and (iii) anticipate which parameter choices are likely to perform well once the indicators are aggregated into the overall score. Correlations are reported as r with two-sided t-tests for $H_0 : \rho = 0$; we refer to $|r| < 0.3$ as weak and $0.3 \leq |r| < 0.6$ as moderate.

Based on the results in Figure 2, the following observations can be made:

- **Heading Indicator**:
  - For α, weak negative trends are common, becoming more negative as γ increases and at longer waypoint spacings.
  - For γ, weak to moderate negative trends dominate, especially for smaller α at longer waypoint spacings.

- **Distance Indicator**:
  - For α, weak negative trends appear for small γ; with large γ, weak positive correlations are seen at 0.5 m. At 2 m, the sign varies with α, becoming positive for very large values.
  - For γ, trends are mostly negative but turn positive for very large α, particularly at intermediate waypoint spacings.
- **Speed Indicator**:
  - For α, positive correlations dominate, stronger for larger initial heading deviations, and are most pronounced for small γ at shorter waypoint spacings.
  - For γ, positive trends occur for small α and short waypoint spacings but tend to become negative at larger α or longer waypoint spacings.

Overall, shorter waypoint distances exhibit weaker and less consistent correlations, whereas longer distances reveal clearer trends shaped by specific α and γ choices. Positive correlations are more evident for smaller γ and small initial heading deviations $\tilde{\theta}_{\text{init}}$, while larger γ, larger d, and larger $\tilde{\theta}_{\text{init}}$ more frequently correspond to negative trends.

Guided by these correlation patterns, we next examine how the candidate parameter sets perform when the indicators are aggregated into the overall score, and how this compares with the resulting ET triggering frequency. Figure 3 illustrates the results of the extensive preliminary simulations: the left-side figures show the calculated overall scores, while the right-side figures show the lowest ET triggering frequency. The overall scores consolidate the three defined indicators, assigning greater weight to the Distance Indicator (favoring shorter traveled distance) than to the Speed and Heading Indicators, as described in (Efimov et al., 2024), Section V. Prioritizing shorter distance reflects the lack of direct control over the robot's trajectory between waypoints and makes the parameter sets suitable for navigation in any environment, including narrow corridors, where the trajectory should remain close to the straight line between waypoints.

From the results of the simulation, we defined two distinct parameter selection modes. The first mode (Table 1) assigns parameter values according to the robot's initial condition before moving to the next waypoint, while the second mode (Table 2) uses a fixed set of values that, irrespective of the initial condition, achieved the highest average overall performance in terms of overall scores and low triggering frequency (best communication reduction). Because, for each mode, two parameter sets achieved the best results with very similar performance, we retained both sets (Parameter Sets 1 and 2) for further evaluation.

Optimized Overall Performance Sets			
d	$\tilde{\theta}_{init}$	α	γ
Short distance ($d < 1\,\text{m}$)	$0° - 45°$	0.6	10
	$45° - 90°$	0.5	1
	$90° - 135°$	1	1
	$135° - 180°$	0.9	1
Medium distance ($1\,\text{m} \leq d < 3\,\text{m}$)	$0° - 45°$	0.8	20
	$45° - 90°$	0.9	5
	$90° - 135°$	1	5
	$135° - 180°$	1	1
Long distance ($3\,\text{m} \leq d$)	$0° - 45°$	1	10
	$45° - 90°$	0.9	20
	$90° - 135°$	0.9	20
	$135° - 180°$	1	10
Optimized Communication Reduction Sets			
d	$\tilde{\theta}_{init}$	α	γ
Short distance ($d < 1\,\text{m}$)	$0° - 45°$	1	10
	$45° - 90°$	0.6	1
	$90° - 135°$	0.1	10
	$135° - 180°$	0.8	1
Medium distance ($1\,\text{m} \leq d < 3\,\text{m}$)	$0° - 45°$	0.2	5
	$45° - 90°$	0.7	20
	$90° - 135°$	0.6	10
	$135° - 180°$	0.5	20
Long distance ($3\,\text{m} \leq d$)	$0° - 45°$	0.9	1
	$45° - 90°$	0.3	20
	$90° - 135°$	0.5	1
	$135° - 180°$	0.3	20

Table 1: Parameter lookup for the ET controller: α and γ selected by waypoint spacing d (short/medium/long) and initial heading deviation $\tilde{\theta}_{\text{init}}$. The upper block lists settings that optimize the average overall performance; the lower block lists settings that minimize the control command triggering frequency, and thus communication load. Values come from preliminary simulations with the Jackal robot in Gazebo.

Optimized Average Overall Performance		
	α	γ
Parameter Set 1	1	1
Parameter Set 2	0.4	20
Optimized Average Communication Reduction		
	α	γ
Parameter Set 1	0.7	20
Parameter Set 2	0.9	1

Table 2: Candidate parameter sets for the ET controller (α and γ) tuned for best average overall performance and tuned for best communication load reduction (via lower control command triggering frequency). These sets are selected independent of waypoint spacing d and initial heading deviation $\tilde{\theta}_{\text{init}}$ in subsequent evaluations.

For the first mode, during operation, the parameters are selected from the lookup table (Table 1) and updated online whenever a new waypoint is assigned, and they remain fixed throughout the traversal of that waypoint.

To further evaluate the performance of the ET controller, a route of total length 21.5 m with ten

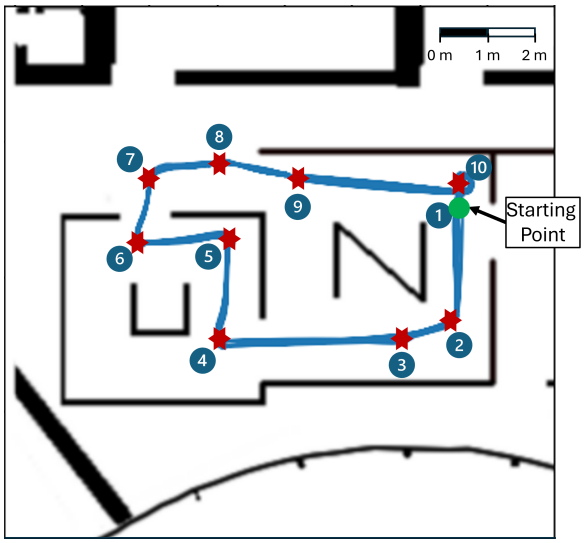

Figure 4: Simulation route (21.5 m) with ten waypoints (stars) and the robot's trajectory over ten loops under the scenario optimizing overall average performance; starting point labeled "1".

waypoints was designed in the simulation (indicated by stars in Figure 4). Waypoint-to-waypoint spacing and the initial heading relative to each goal were varied to elicit diverse motions. Average performance along this trajectory was assessed using the ET parameter sets previously derived in Tables 1 and 2.

Starting from the "Starting Point" (labeled 1 in Figure 4), the robot was programmed to traverse all waypoints clockwise and return to the start. The event-triggered control framework (Algorithm 1) specifies the parameter updates, triggering condition, and control-signal generation. Simulations were conducted under two scenarios: one prioritizing overall performance and one minimizing communication overhead. For each scenario, two parameter modes were tested: (i) a condition-based lookup updated at each waypoint (Table 1); and (ii) fixed candidate sets that achieved the best average overall results across initial headings and waypoint spacings (Table 2).

Each scenario was executed ten times, and the results are reported in Figure 5, with error bars indicating variability across runs. For baseline comparison, the same route was simulated using a periodic controller operating at 5 Hz. Figure 4 illustrates the robot's trajectory under the scenario optimizing overall average performance. Table 3 summarizes the average control command triggering frequency for the different parameter sets. The results show that, with appropriately chosen parameters, the control command triggering frequency was reduced by up to 80% in both scenarios (prioritizing overall performance and minimizing communication overhead).

From Figure 5, it can be observed that the proposed ET strategy introduces minor trade-offs, such as slightly reduced speed and trajectory smoothness;

Algorithm 1 Event-Triggered Control Framework

Require:
- Current robot state $X(t)$
- Current desired waypoint X^d
- Online update policy for control parameters $[\alpha, \gamma]$
- Previously frozen control $U(t_k)$

while mission is active **do**
  if a new waypoint X^d is received **then**
    Update parameters $[\alpha, \gamma]$
  end if
  Compute instantaneous control $U(t)$ using (5)
  if $t = t_{k+1}$ from (9) **then**
    $k \leftarrow k + 1$
    Compute new control $U(t_k)$ using (10)
    Output $U(t_k)$
  else
    Keep previous frozen control $U(t_k)$
  end if
end while

Remark: Once a new waypoint is received, a coordinate transformation can be applied to place it at the origin of the coordinate system. Intuitively, this means that the waypoint-tracking problem can always be reformulated as a regulation problem, where the task reduces to driving the robot's pose to the origin.

Parameter Set	ET controller Average Triggering Frequency
Optimized Average Overall Performance - Parameter Set 1	2.83 Hz
Optimized Average Overall Performance - Parameter Set 2	1.02 Hz
Optimized Overall Performance Sets	1.88 Hz
Optimized Average Comm. Reduction - Parameter Set 1	1.01 Hz
Optimized Average Comm. Reduction - Parameter Set 2	1.17 Hz
Optimized Communication Reduction Set	1.03 Hz

Table 3: Average ET triggering frequency (Hz) in simulation for each parameter selection mode and candidate set, over a 21.5 m route with 10 waypoints; each scenario repeated 10 times. Lower frequency indicates fewer control command transmissions.

however, these degradations remain within acceptable bounds. Performance degradation is, as can be expected, less pronounced when parameters are selected to prioritize overall performance rather than reducing the control command triggering frequency.

The results also indicate that when parameter sets are derived from the robot's initial conditions (lookup

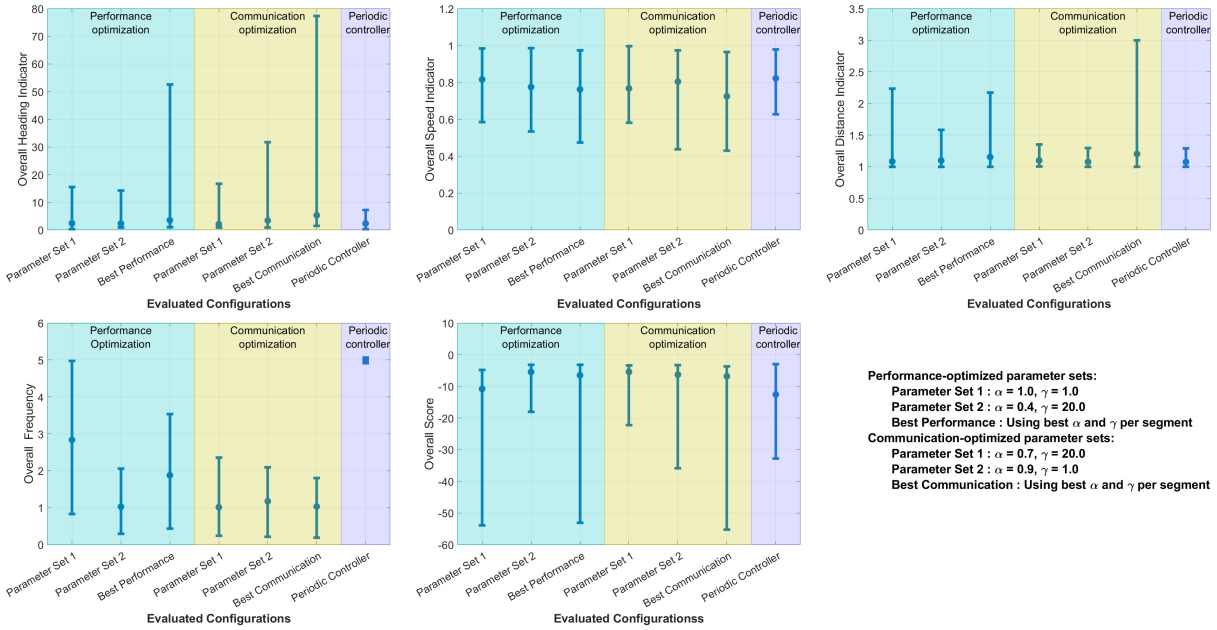

Figure 5: Simulation results showing the effect of ET controller parameter settings on the performance indicators and the control command triggering frequency. The triggering frequency indicates the communication load; lower values indicate reduced load.

mode), as obtained in the preliminary simulations, overall performance tends to decline along the complex route. This effect can be attributed to the sparsity of the preliminary condition grid, particularly with respect to the initial heading deviation $\tilde{\theta}_{\text{init}}$, which strongly influences the suitability of the selected ET parameters.

Accordingly, it is more effective to employ a parameter set that yields the best average overall performance, irrespective of the initial condition within the tested range, rather than relying on condition-specific parameter selection.

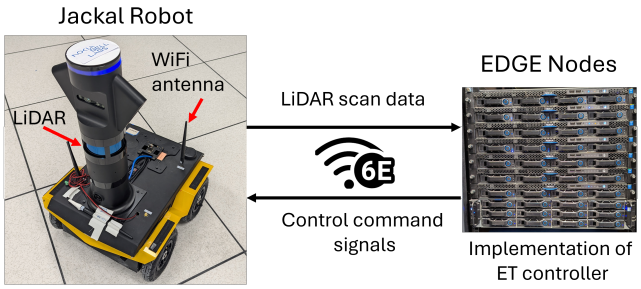

Figure 6: Experimental setup with the Jackal robot and the edge cloud.

6. Event-triggered experimental results

To evaluate the performance of the proposed method, experiments were conducted in the laboratory in Massy, France. A Clearpath Jackal, the same platform as in simulation, was used with the same LiDAR-based localization algorithm (Figure 6). The experimental route, designed for this study, measured 21.8 m and comprised eight waypoints (Figure 7), approximately matching the simulated route length. Based on the prior simulation results, parameter sets selected from the lookup table according to the initial condition (Table 1) and condition-independent parameter sets that achieved the best average overall performance (Table 2) were used in the experiments.

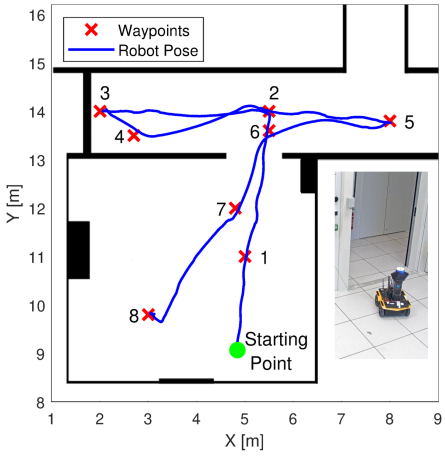

Figure 7: Experimental route (21.8 m) with eight waypoints and an example trajectory of the robot under the performance-prioritized setting (Parameter Set 2). Right: snapshot shows the robot moving from waypoint 6 → 7.

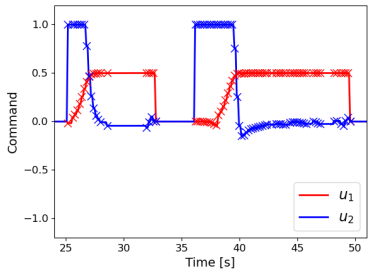

(a) Performance optimization - Parameter Set 1

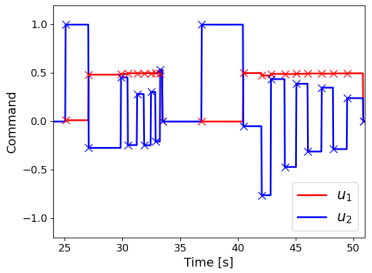

(b) Performance optimization - Parameter Set 2

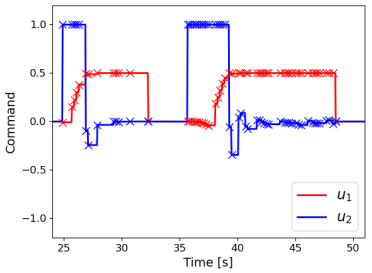

(c) Best performance optimization parameters

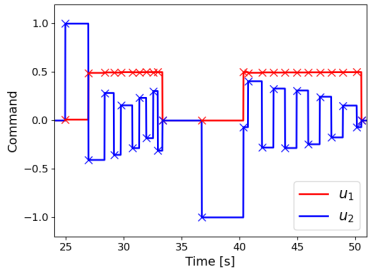

(d) Communication optimization - Parameter Set 1

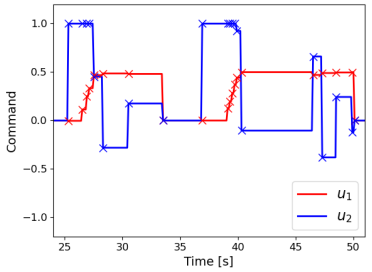

(e) Communication optimization - Parameter Set 2

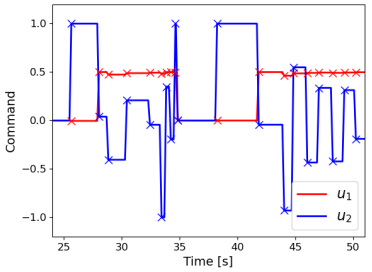

(f) Best communication optimization parameters

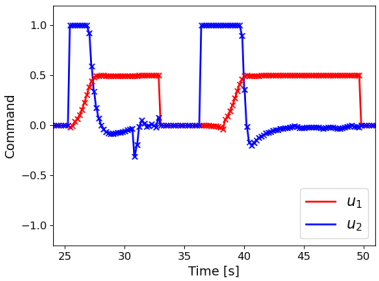

(g) Periodic controller

Figure 8: Control command velocities over a part of an experiment round. Subfigures (a)-(c) correspond to command velocities with performance-prioritized parameter tuning, (d)-(f) to command velocities with frequency-prioritized parameter tuning, and (g) to the periodic controller at 5 Hz. Cross markers indicate triggering instances. Note that u_1 (linear velocity) and u_2 (angular velocity) share the same y-axis but are expressed in different units (m/s and rad/s, respectively).

Consistent with the simulation setup, two scenarios were considered: one prioritizing overall performance and one minimizing communication. A periodic controller operating at 5 Hz served as a baseline. Each experiment consisted of five loops of the route. Starting from the "Starting Point" (Figure 7), the robot traversed all waypoints in order. Figure 7 illustrates the waypoints and a representative trajectory under the average overall performance-prioritized setting (Parameter Set 2 in Table 2).

Figure 8 illustrates the control command velocities recorded over a portion of a run. As observed, the number of control commands, and thus the communication load, is significantly reduced under the event-triggered controller relative to the periodic baseline. When parameters are selected to prioritize controller performance (via the lookup table or the candidate sets identified for optimized average overall performance), the control signals transmitted to the robot remain closer to the nominal values of the periodic controller. Conversely, when parameters are chosen to minimize the control command triggering frequency, overall performance degrades modestly, with more oscillatory and irregular command velocities.

Aggregated experimental results are shown in Figure 9, and the average control command triggering frequencies are summarized in Table 4. With appropriate parameter choices, the control command triggering frequency was reduced by up to 80% in both scenarios (performance-prioritized and communication-optimization), while maintaining acceptable tracking performance. These results demonstrate the effectiveness of the proposed method in a real experimental setup.

As expected, the triggering frequencies in the physical environment were slightly higher than in simulation for the same parameter settings. This increase is attributed to the inherent noise and disturbances present under real-world conditions.

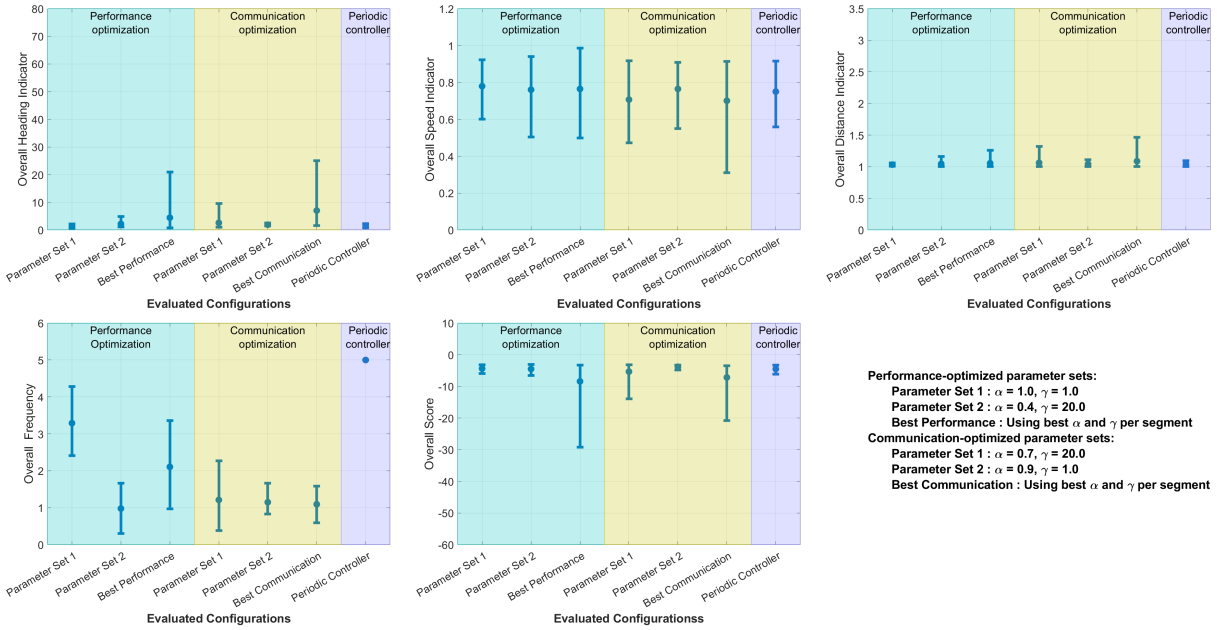

Figure 9: Comparative experimental results on the Jackal robot showing the effect of ET controller parameter settings on the performance indicators and the control command triggering frequency. The triggering frequency indicates the communication load; lower values indicate reduced load.

Parameter Sets	ET controller Average Triggering Frequency
Optimized Average Overall Performance - Parameter Set 1	3.3 Hz
Optimized Average Overall Performance - Parameter Set 2	1.14 Hz
Optimized Overall Performance Set	2.1 Hz
Optimized Average Comm. Reduction - Parameter Set 1	1.15 Hz
Optimized Average Comm. Reduction - Parameter Set 2	1.21 Hz
Optimized Communication Reduction Set	1.09 Hz

Table 4: Average ET triggering frequency (Hz) in physical experiments with the Jackal robot over a 21.8 m route with 8 waypoints using LiDAR-based localization, with the same parameter-selection modes and candidate sets as in simulation. A periodic 5 Hz controller is included as baseline; lower frequency indicates fewer control command transmissions.

Nevertheless, regulation performance and triggering frequency remained comparable between physical and simulated experiments, demonstrating the robustness of the proposed method. In addition, the standard deviation of the measured data was consistently low across experiments, indicating stable behavior and reliable control performance under varying conditions.

7. Conclusion

This work addressed the robust stabilization problem of a wheeled mobile robot modeled with unicycle dynamics. By relaxing the strict regulation objective, a bounded control law was synthesized, guaranteeing global convergence of the robot's position to the origin in the x and y coordinates (i.e., the desired waypoint) independently of disturbances in the control channels. The stability properties of the resulting closed-loop nonlinear system were established using a simple strict Lyapunov function.

To facilitate integration of the proposed control strategy within a networked navigation framework, such as a centralized planner or supervisor, an event-triggered implementation of the algorithm was developed following the method in (Postoyan et al., 2015b). The influence of controller tuning on both regulation performance and triggering behavior was systematically examined. Simulation-based parameter tuning showed that event-triggered regulation can reduce communication between the robot and the controller by up to 80% with negligible impact on overall system performance. These results were validated in both simulation and physical experiments, confirming the practical feasibility of the approach.

Future work will consider dynamic and adaptive adjustment of parameters during transitions between waypoints, as well as further investigation of robustness in the presence of communication delays.

References

Aicardi, M., Casalino, G., Bicchi, A., Balestrino, A., 1995. Closed loop steering of unicycle like vehicles via Lyapunov techniques. IEEE Robotics & Automation Magazine 2, 27–35. doi:10.1109/100.388294.

Astolfi, A., 1996. Discontinuous control of nonholonomic systems. Systems & Control Letters 27, 37–45. doi:https://doi.org/10.1016/0167-6911(95)00041-0.

Brockett, R., 1983. Differential Geometric Control Theory. Birkhäuser, Boston. chapter Asymptotic Stability and Feedback Stabilization. pp. 181–208.

Censi, A., 2008. An icp variant using a point-to-line metric, in: 2008 IEEE International Conference on Robotics and Automation, pp. 19–25. doi:10.1109/ROBOT.2008.4543181.

De Luca, A., Oriolo, G., Samson, C., 1998. Robot Motion Planning and Control. Springer. chapter Feedback control of a nonholonomic car-like robot. pp. 171–253. doi:10.1007/BFb0036073.

Dixon, W., Dawson, D.M., Zergeroglu, E., Behal, A., 2001. Nonlinear Control of Wheeled Mobile Robots. Lecture Notes in Control and Information Sciences, Springer-Verlag, London.

Do, K., 2013. Bounded controllers for global path tracking control of unicycle-type mobile robots. Robotics and Autonomous Systems 61, 775–784. doi:https://doi.org/10.1016/j.robot.2013.04.014.

Efimov, D., Khalili, M., Liu, S., 2024. Global event-triggered regulation of unicycle dynamics by bounded control, in: 2024 Conference on Decision and Control (CDC), IEEE.

Evers, W.J., Nijmeijer, H., 2006. Practical stabilization of a mobile robot using saturated control, in: Proceedings of the 45th IEEE Conference on Decision and Control, San Diego. pp. 2394–2399.

Fox, D., Burgard, W., Thrun, S., 1997. The dynamic window approach to collision avoidance. IEEE Robotics and Automation Magazine 4, 23–33. doi:10.1109/100.580977.

Girard, A., 2015. Dynamic triggering mechanisms for event-triggered control. IEEE Transactions on Automatic Control 60, 1992–1997. doi:10.1109/TAC.2014.2366855.

Jiang, Z.P., Nijmeijer, H., 1997. Tracking Control of Mobile Robots: A Case Study in Backstepping. Automatica 33, 1393–1399.

Khalil, H.K., 2002. Nonlinear Systems Third Edition. Prentice Hall.

Kolmanovsky, I., McClamroch, N., 1995. Developments in nonholonomic control problems. IEEE Control Systems Magazine 15, 20–36. doi:10.1109/37.476384.

Kostic, D., Adinandra, S., Caarls, J., Van De Wouw, N., Nijmeijer, H., 2009. Collision-free tracking control of unicycle mobile robots, in: Proceedings of the 48th IEEE Conference on Decision and Control held jointly with the 2009 28th Chinese Control Conference, Shanghai. pp. 5667–5672.

Kuwata, Y., Teo, J., Fiore, G., Karaman, S., Frazzoli, E., How, J.P., 2009. Real-time motion planning with applications to autonomous urban driving. IEEE Transactions on Control Systems Technology 17, 1105–1118. doi:10.1109/TCST.2008.2012116.

Lamnabhi-Lagarrigue, F., Annaswamy, A., Engell, S., Isaksson, A., Khargonekar, P., Murray, R.M., Nijmeijer, H., Samad, T., Tilbury, D., Van den Hof, P., 2017. Systems and Control for the future of humanity, research agenda: Current and future roles, impact and grand challenges. Annual Reviews in Control 43, 1–64.

Lemmon, M., 2010. Networked Control Systems. Springer. chapter Event-Triggered Feedback in Control, Estimation, and Optimization. pp. 293–358. doi:10.1007/978-0-85729-033-5_9.

Martínez, E.A., Ríos, H., Mera, M., 2021. Robust tracking control design for unicycle mobile robots with input saturation. Control Engineering Practice 107, 104676. doi:https://doi.org/10.1016/j.conengprac.2020.104676.

d'Andréa Novel, B., Campion, G., Bastin, G., 1995. Control of nonholonomic wheeled mobile robots by state feedback linearization. The International Journal of Robotics Research 14, 543–559. doi:10.1177/027836499501400602.

Postoyan, R., Bragagnolo, M.C., Galbrun, E., Daafouz, J., Nešić, D., Castelan, E.B., 2015a. Event-triggered tracking control of unicycle mobile robots. Automatica 52, 302–308. doi:https://doi.org/10.1016/j.automatica.2014.12.009.

Postoyan, R., Tabuada, P., Nešić, D., Anta, A., 2015b. A framework for the event-triggered stabilization of nonlinear systems. IEEE Transactions on Automatic Control 60, 982–996. doi:10.1109/TAC.2014.2363603.

Tabuada, P., 2007. Event-Triggered Real-Time Scheduling of Stabilizing Control Tasks. IEEE Transactions on Automatic Control 52, 1680–1685.

Tatikonda, S., Mitter, S., 2004. Control under communication constraints. IEEE Transactions on Automatic Control 49, 1056–1068. URL: http://ieeexplore.ieee.org/document/1184366/.

de Wit, C.C., Khennouf, H., Samson, C., Sørdalen, O.J., 1994. Recent Trends in Mobile Robots. World Scientific. chapter Nonlinear control design for mobile robots. pp. 121–156. doi:10.1142/9789814354301_0005.

Zhang, P., Liu, T., Jiang, Z.P., 2023. Tracking control of unicycle mobile robots with event-triggered and self-triggered feedback. IEEE Transactions on Automatic Control 68, 2261–2276. doi:10.1109/TAC.2022.3173932.